01 Jan 1989

Adiabatic Shear Banding In Plane Strain Problems

R. C. Batra
Missouri University of Science and Technology

De Shin Liu

Recommended Citation

R. C. Batra and D. S. Liu, "Adiabatic Shear Banding In Plane Strain Problems," *Journal of Applied Mechanics, Transactions ASME*, vol. 56, no. 3, pp. 527 - 534, American Society of Mechanical Engineers, Jan 1989.
The definitive version is available at https://doi.org/10.1115/1.3176122

Adiabatic Shear Banding in Plane Strain Problems

R. C. Batra
Mem. ASME

De-Shin Liu

Department of Mechanical and Aerospace Engineering and Engineering Mechanics, University of Missouri-Rolla, Rolla, Mo. 65401-0249

Plane strain thermomechanical deformations of a viscoplastic body are studied with the objective of analyzing the localization of deformation into narrow bands of intense straining. Two different loadings, namely, the top and bottom surfaces subjected to a prescribed tangential velocity, and these two surfaces subjected to a preassigned normal velocity, are considered. In each case a material defect, flaw, or inhomogeneity is modeled by introducing a temperature bump at the center of the specimen. The solution of the initial boundary value problem by the Galerkin-Adams method reveals that the deformation eventually localizes into a narrow band aligned along the direction of the maximum shearing strain. For both problems, bands of intense shearing appear to diffuse out from the center of the specimen.

1 Introduction

Adiabatic shear banding is the name given to a localization phenomenon that occurs during high-rate plastic deformation such as machining, explosive forming, shock-impact loading, ballistic penetration, fragmentation, ore crushing, impact tooling failure, and metal shaping and forming processes. The localization of the deformation has been observed in steels, nonferrous metals, and polymers. Practical interest in the phenomenon derives from the fact that progressive shearing on an intense shear band provides an undesirable mode of material resistance to imposed deformations, and the bands are often precursors to shear fractures. Of the many processes just stated in which adiabatic shear bands have been found to occur, flat sheet rolling and certain forging operations can be modeled as plane strain operations.

Since the time Zener and Hollomon (1944) recognized the destabilizing effect of thermal softening in reducing the slope of the stress-strain curve in nearly adiabatic deformations, there have been numerous studies aimed at delineating material parameters that enhance or retard the initiation and growth of adiabatic shear bands. Most of the effort has been concentrated in analyzing the simple shearing problem. Clifton (1980) and Bai (1981) studied the growth of infinitesimal periodic perturbations superimposed on a body deformed by a finite amount in simple shear. Burns (1985) used a dual asymptotic expansion to account for the time dependence of the homogeneous solution in the analysis of the growth of superimposed periodic perturbations. Merzer (1982) used the constitutive relation proposed by Bodner and Partom (1975) to study the problem of twisting of a thin tubular specimen having a notch in its periphery. He concluded that the band width depends upon the thermal conductivity. Wu and Freund (1984) used a different material model and studied wave propagation in an infinite medium. They concluded that the thermal conductivity has essentially no effect on the width of a shear band. Other works analyzing the initiation and growth of adiabatic shear bands include those due to Clifton et al. (1984), Wright and Batra (1985), Wright and Walter (1987), Batra (1987), and Batra and Kim, (1989). Rogers (1979, 1983) and Timothy (1987) have reviewed various aspects of adiabatic shear banding, especially from a materials point of view.

Experimental studies dealing with adiabatic shear banding include those of Zener and Hollomon (1944), Moss (1981), Costin et al. (1979), Lindholm and Johnson (1983), and Marchand and Duffy (1988). Marchand and Duffy have given a detailed history of the temperature and strain fields within a band.

Needleman (1989) has recently studied the initiation and growth of shear bands in plane strain deformations of viscoplastic materials. He studied a purely mechanical problem and approximated the effect of thermal softening by assuming that the stress-strain curve has a peak in it. He modeled a material inhomogeneity by assuming that the flow stress for a small amount of material near the center of the block was less than that of the surrounding material. We study herein the thermomechanical plane strain deformations of a thermally softening viscoplastic solid and model the material inhomogeneity by introducing a temperature bump at the center of the block. The block boundaries are assumed to be perfectly insulated. Two different deformation states, namely, that of a simple shearing of the block, and the block deformed in simple compression are analyzed. In each case a shear band develops along the direction of maximum shearing strain. Whereas the deformation localizes at an average compressive strain of 0.059 when the block is deformed in compression, the average shear strain equals 0.227 when the block is deformed in simple shear.

Contributed by the Applied Mechanics Division of THE AMERICAN SOCIETY OF MECHANICAL ENGINEERS for presentation at the Winter Annual Meeting, San Francisco, Calif., December 10–15, 1989.

Discussion on this paper should be addressed to the Editorial Department, ASME, United Engineering Center, 345 East 47th Street, New York, N.Y. 10017, and will be accepted until two months after final publication of the paper itself in the JOURNAL OF APPLIED MECHANICS. Manuscript received by the ASME Applied Mechanics Division, July 29, 1988; final revision, November 18, 1988.

Paper No. 89-WA/APM-16.

2 Formulation of the Problem

We use a fixed set of rectangular Cartesian coordinate axes to describe the thermomechanical deformations of the body. In terms of the referential description the governing equations are

$$(\rho J)^{\cdot} = 0, \tag{1}$$

$$\rho_0 \dot{v}_i = T_{i\alpha,\alpha}, \tag{2}$$

$$\rho_0 \dot{e} = -Q_{\alpha,\alpha} + T_{i\alpha} v_{i,\alpha}, \tag{3}$$

and a suitable set of initial and boundary conditions. Equation (1) expresses the balance of mass, (2) the balance of linear momentum, and (3) the balance of internal energy. In these equations, ρ is the current mass density, ρ_0 the mass density in the reference configuration, J is the determinant of the deformation gradient, v_i the velocity of a material particle in the x_i direction, Q_α the heat flux, e the specific internal energy, $T_{i\alpha}$ the first Piola-Kirchoff stress tensor, a superimposed dot stands for the material time derivative, and a comma followed by an index $\alpha(j)$ implies partial differentiation with respect to $X_\alpha(x_j)$. Also $\mathbf{x}$ denotes the present position of a material particle that occupied the place $\mathbf{X}$ in the reference configuration, and a repeated index implies summation over the range of the index. For plane strain deformations, $x_3 = X_3$ and the indices i and α take on values 1 and 2.

For the constitutive relations we take

$$\boldsymbol{\sigma} = -p(\rho)\mathbf{1} + 2\mu\mathbf{D}, \; T_{i\alpha} \equiv \frac{\rho_0}{\rho} X_{\alpha,j}\sigma_{ij}, \tag{4}$$

$$2\mu = \frac{\sigma_0}{\sqrt{3I}}(1-\nu\theta)(1+bI)^m, \; 2D_{ij} = v_{i,j} + v_{j,i}, \tag{5}$$

$$I^2 = \frac{1}{2}\mathrm{tr}\tilde{\mathbf{D}}^2, \; \tilde{\mathbf{D}} = \mathbf{D} - \frac{1}{3}(\mathrm{tr}\mathbf{D})\mathbf{1}, \tag{6}$$

$$p(\rho) = B\left(\frac{\rho}{\rho_0} - 1\right), \tag{7}$$

$$Q_\alpha = -k\theta_{,\alpha}, \tag{8}$$

$$\dot{e} = c\dot{\theta} + \dot{\rho}p(\rho)/(\rho\rho_0). \tag{9}$$

Here, σ_0 is the yield stress in simple tension or compression, ν is the coefficient of thermal softening, parameters b and m represent the strain rate sensitivity of the material, B may be thought of as the bulk modulus, k is the thermal conductivity, and c the specific heat. Equation (7) is a part of the Tillotson (1962) equation wherein the dependence of the pressure upon the changes in temperature has not been considered, and equation (8) is the Fourier law of heat conduction.

Defining $\mathbf{s}$ as

$$\mathbf{s} = \boldsymbol{\sigma} + \left(p - \frac{2\mu}{3}\mathrm{tr}\mathbf{D}\right)\mathbf{1}, \tag{10}$$

$$= 2\mu\tilde{\mathbf{D}}, \tag{11}$$

equations (4) and (5) give

$$\left(\frac{1}{2}\mathrm{trs}^2\right)^{1/2} = \frac{\sigma_0}{\sqrt{3}}(1-\nu\theta)(1+bI)^m, \tag{12}$$

which can be viewed as a generalized von Mises yield surface when the flow stress (given by the right-hand side of (12)) at a material particle depends upon its strain rate and temperature. The linear dependence of the flow stress upon the temperature change has been observed by Bell (1968), Lindholm and Johnson (1983), and Lin and Wagoner (1986). A constitutive relation similar to equation (4) has been used by Zienkiewicz et al. (1981) in analyzing the extrusion problem, by Batra (1988) in studying the steady-state penetration of a viscoplastic target by a rigid cylindrical penetrator, and by Batra and Lin (1989) in studying the steady-state axisymmetric deformations of a cylindrical viscoplastic rod upset at the bottom of a hemispherical rigid cavity. Equation (4) may be interpreted as a constitutive relation for a non-Newtonian fluid whose viscosity μ depends upon the strain rate and temperature.

We introduce nondimensional variables as follows:

$$\bar{\boldsymbol{\sigma}} = \boldsymbol{\sigma}/\sigma_0, \; \bar{p} = p/\sigma_0, \bar{\mathbf{s}} = \mathbf{s}/\sigma_0, \bar{\mathbf{v}} = \mathbf{v}/v_0, \; \bar{t} = tv_0/H, \; \bar{\mathbf{T}} = \mathbf{T}/\sigma_0,$$
$$\bar{\mathbf{x}} = \mathbf{x}/H, \; \bar{\theta} = \theta/\theta_0, \; \bar{b} = b\frac{v_0}{H}, \; \bar{\nu} = \nu\theta, \; \bar{\rho} = \rho/\rho_0, \; \bar{\mathbf{X}} = \mathbf{X}/H,$$
$$\delta = \rho_0 v_0^2/\sigma_0, \; \beta = k/(\rho_0 c v_0 H), \; \theta_0 = \sigma_0/(\rho_0 c), \; \bar{B} = B/\sigma_0. \tag{13}$$

Here, $2H$ is the height of the block, v_0 is the imposed velocity on the top and bottom surfaces, and ρ_0 is the mass density in the unstressed reference configuration. Substituting from equations (4) through (9) into the balance laws (1) through (3), rewriting these in terms of nondimensional variables, denoting the partial differentiation with respect to $\bar{x}_i(\bar{X}_\alpha)$ by a comma followed by an index $i(\alpha)$, material differentiation with respect to t by a superimposed dot, and dropping the superimposed bars, we arrive at the following set of equations:

$$\dot{\rho} + \rho v_{i,i} = 0, \tag{14}$$

$$\delta\dot{v}_i = T_{i\alpha,\alpha}, \tag{15}$$

$$\dot{\theta} = \beta\theta_{,\alpha\alpha} + [1/(\sqrt{3I}\rho)](1-\nu\theta)(1+bI)^m D_{ij}D_{ij}, \tag{16}$$

$$\boldsymbol{\sigma} = -B(\rho-1)\mathbf{1} + \frac{1}{\sqrt{3I}}(1+bI)^m(1-\nu\theta)\mathbf{D}. \tag{17}$$

It is simpler to state boundary conditions for the specific problem studied. We analyze plane strain thermomechanical deformations of an initially-square block of dimension $2H \times 2H$. The $X_1 - X_2$ plane, with the origin of the coordinate system located at the center of the block, is taken as the plane of deformation. For the simple shearing problem the boundary conditions are taken to be

$$v_1 = \pm f(t), \; v_2 = 0, \; Q_\alpha N_\alpha = 0 \text{ at } X_2 = \pm H, \tag{18}$$

$$n_i T_{i\alpha} N_\alpha = 0, \; e_i T_{i\alpha} N_\alpha = h(t), \; Q_\alpha N_\alpha = 0 \text{ at } X_1 = \pm H, \tag{19}$$

where $\mathbf{n}$ is a unit outward normal and $\mathbf{e}$ is a unit vector tangent to the surface in the present configuration and $\mathbf{N}$ is a unit outward normal in the reference configuration. Equations (18) and (19) imply that the boundaries of the block are perfectly insulated, the top and bottom faces are placed in a hard loading device and are subjected to a known velocity field. On the other two faces of the block, zero normal tractions are assigned and the tangential tractions are such as to equilibrate the ones acting on the top and bottom faces. For a known function f, the values of h depend upon the constitutive relation for the material of the block, and hence, are not known *a priori*. As discussed in Section 3, we solve the resulting system of equations iteratively and find h as a part of the solution of the problem.

For the simple compression problem, we restrict ourselves to the deformations that remain symmetric about both $X_1 = 0$ and $X_2 = 0$. The boundary conditions for the quadrant analyzed numerically are

$$v_1 = 0, \; T_{21} = 0, \; Q_1(Ku)_1 = 0, \text{ at } x_1 = X_1 = 0, \tag{20}$$

$$v_2 = 0, \; T_{12} = 0, \; Q_2 = 0, \text{ at } x_2 = X_2 = 0, \tag{21}$$

$$T_{i\alpha}N_\alpha = 0, \; Q_\alpha N_\alpha = 0, \text{ at } X_1 = H, \tag{22}$$

$$v_2 = U(t), \; e_i T_{i\alpha} N_\alpha = 0, \; Q_\alpha N_\alpha = 0, \text{ at } X_2 = H. \tag{23}$$

That is boundary conditions resulting from the assumed symmetry of deformations are applied to the left and bottom faces, the right face of the block is taken to be traction free, and a prescribed normal velocity field and zero tangential tractions are applied on the top face. All four sides of the block are assumed to be perfectly insulated.

In each of the two problems, a material inhomogeneity or flaw is modeled by adding a temperature bump at the center of the block to the temperature field that corresponds to a homogeneous deformation of the block.

3 Finite Element Formulation of the Problem

In order to avoid having to deal with a severely distorted finite element mesh within the region of localization of the deformation, we employ an updated Lagrangian formulation. Thus to find the deformed shape of the body at time $t+\Delta t$, we take the configuration at time t as the reference configuration, and denote the region occupied by the body at time t by Ω. At subsequent times the current locations of the nodes are computed and Ω equals the union of the 9-noded quadrilateral elements obtained by joining these nodes. No attempt was made to ensure that when the deformation localizes, the element sides will be aligned along the direction of the maximum shearing strain (cf., Needleman, 1989). However, for the simple shearing problem, the element sides are so aligned at the initiation of the localization of the deformation.

We first rewrite equations (14)–(16) so that terms involving the partial derivative with respect to time t only are on the left-hand side and then use the Galerkin method and the lumped mass matrix (e.g., see Hughes (1987)) to derive the following semi-discrete formulation of the problem.

$$\dot{\mathbf{d}} = \mathbf{F}(\mathbf{d}, \delta, \beta, b, m, \nu). \tag{24}$$

Here, $\mathbf{d}$ is the vector of nodal values of the mass density, two components of the velocity, and the temperature. Thus the total number of unknowns or the number of components of $\mathbf{d}$ equals four times the number of nodes. The vector-valued function $\mathbf{F}$ on the right-hand side of equation (24) is a nonlinear function of $\mathbf{d}$ and of the material parameters δ, β, b, m, and ν. For a given set of initial values of ρ, $\mathbf{v}$ and θ, one can deduce the initial conditions on $\mathbf{d}$. The nonlinear coupled set of ordinary differential equations (24) are solved by using the backward-difference Adams method included in the IMSL subroutine LSODE. During the solution of these equations, the tangential traction on the current position of the faces $X_1 = \pm H$ as determined from the immediately preceding solution, is applied. The subroutine LSODE has the option to use the modified Gear method appropriate for stiff equations. This could not be used because of the limited core storage available on the local FPS164 processor attached to IBM 4381 computer. For the Adams method, the subroutine LSODE adjusts the size of the time increment adaptively until it can compute a solution of the nonlinear equations (24) to the prescribed accuracy.

4 Computation and Discussion of Results

We took the following values of various material and geometric parameters to compute numerical results.

$$b = 10{,}000 \text{ sec}, \nu = 0.0222^\circ\text{C}^{-1}, \sigma_0 = 333\text{MPa}, m = 0.025,$$

$$k = 49.22\ \text{Wm}^{-1}{}^\circ\text{C}^{-1}, c = 473\text{Jkg}^{-1}{}^\circ\text{C}^{-1}, \rho_0 = 7{,}800\ \text{kgm}^{-3},$$

$$B = 128\text{GPa}, H = 5\text{mm}, v_0 = 25\ \text{msec}^{-1}. \tag{25}$$

For these choices, $\theta_0 = 89.6^\circ\text{C}$, the nondimensional melting temperature equals 0.5027, and the overall applied strain rate is 5000 sec^{-1}. We assigned a rather large value to the thermal softening coefficient ν to reduce the CPU time required to solve the problem.

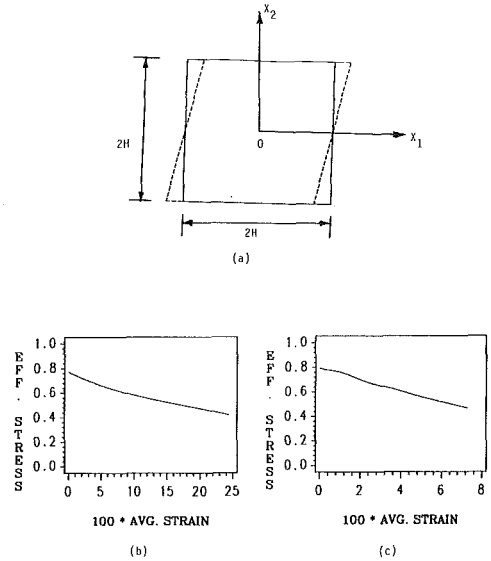

Fig. 1 (a) The shape of the block in the reference configuration and after it has been deformed uniformly in simple shear, (b) Stress-strain curve in simpler shear, and (c) Stress-strain curve in simple compression

Figure 1 depicts the block in the undeformed reference configuration and its shape after it has been deformed uniformly in simple shear. Also plotted are the stress strain curves for the material defined by parameters (25) when the block is deformed in simple shear and simple compression. It is obvious that the softening caused by the heating of the material exceeds the hardening due to strain rate effects right from the beginning. This is due to the rather high value of the thermal softening coefficient assumed for the material of the block. Once the deformation begins to localize, equations (24) become stiff and the maximum size of the time step one can use and still integrate these equations to the desired degree of accuracy becomes extremely small. Ideally, one should then use the Gear method. But, as stated previously, we could not do so because of the limited core storage available. The results presented and discussed next are up to the moment when the deformation has localized into a narrow band. Results computed earlier for the one-dimensional problem (Batra (1987), Batra and Kim (1989), and Wright and Walter (1987)) suggest that the presently computed results represent essentially all of the salient features of the localization of the deformation. We first discuss results for the simple shearing problem, and then the compression problem.

(a) Results for the Simple Shearing Problem. The square region in the configuration at time $t=0$ is divided into 16×16 uniform 9-noded square elements. The velocity field

$$v_1 = x_2, v_2 = 0 \tag{26}$$

that corresponds to steady shearing of the block, and the temperature field

$$\theta = 0 \tag{27}$$

are taken as the initial conditions at time $t=0$, and for the boundary conditions we take

$$f(t) = 1.0, t > 0.$$

Thus, the effect of initial transients is assumed to have died out. This reduces the computational effort required without altering noticeably the computed results. Subsequent calculations with zero-initial conditions for v_1, v_2, and θ have given essentially similar results.

At time $t=0$, a temperature bump given by

$$\Delta\theta = 0.2(1-r^2)^9 \exp(-5r^2),\ r^2 = X_1^2 + X_2^2 \qquad (28)$$

was introduced and the resulting initial boundary value problem solved. The temperature bump (28) simulates a material inhomogeneity or defect; the height of the bump represents, in some sense, the strength of the singularity. Without the temperature bump or some other mechanism to make the deformation nonhomogeneous, the block will undergo unlimited simple shearing deformations and no localization of the deformation will occur. We note that other ways to model an initial imperfection in the body include having a notch (Clifton et al., 1984) and a small region with a slightly lower value of the yield stress (Needleman, 1989). For strain hardening materials the introduction of a temperature bump, a notch or a softer region does not, in general, lead to the localization of the deformation. The average strain at which a shear band forms depends upon, among other factors, the amplitude and shape of the temperature bump.

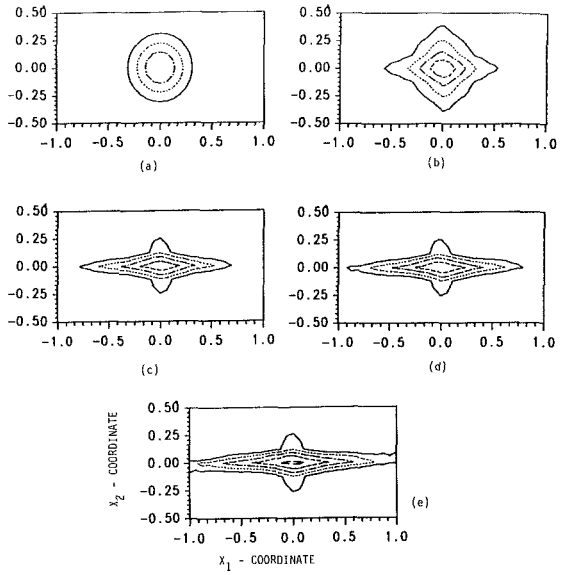

Fig. 2 Isotherms plotted in the reference configuration at different values of the average strain for simple shearing deformations of the block; (a) $\gamma_{avg}=0$, $\theta_{max}=0.2$, — 0.15, • • • • 0.10, —•—•—• 0.15, 0.05, (b) $\gamma_{avg}=0.13$, $\theta_{max}=0.344$, — 0.15, • • • • 0.20, —•—•—• 0.25, - - - - 0.30, (c) $\gamma_{avg}=0.208$, $\theta_{max}=0.441$, — 0.25, • • • • 0.30, —•—•—• 0.35, - - - - 0.40, — — — 0.45, (d) $\gamma_{avg}=0.215$, $\theta_{max}=0.449$ (see part (c) for values of θ corresponding to different curves), and (e) $\gamma_{avg}=0.227$, $\theta_{max}=0.463$ (see part (c) for values of θ corresponding to different curves)

Figure 2 shows isotherms in the reference configuration of the block at four different values of the average strain γ_{avg}. Initially, these isotherms look elliptical because of the different choice of scales along the horizontal and vertical axes. The temperature bump is symmetrical in x_1 and x_2. A reason for selecting different scales along the two axes is that the isotherms eventually flaten out and spread to the vertical boundaries of the block. Thus, larger scale is chosen along the vertical axis to decipher these isotherms. The initial temperature equals 0.20 only at the origin. At an average strain of 13 percent, the isotherms have changed shape; those for a lower temperature look like a rhombus and the ones for the higher temperature resemble closed polygons. Because of the plastic working and zero heat flux boundary conditions the temperature rises everywhere. The heat is continuously being conducted outwards from the central hotter region. Near the corners of the block deformation is nonhomogeneous (e.g., see Fig. 5) and the temperature rise there is more than that at other points except possibly near the center of the block. The nonhomogeneity of the deformation near the corners is a numerical artifact rather than due to the physics of the problem. The use of a very fine mesh should reduce the effect considerably, but a mesh finer than the one employed here could not be used because of the limited core storage available. Once the deformation begins to localize, the temperature rise within the band is significantly more than what it is elsewhere. The temperature contours at average strains of 20.8 percent, 21.5 percent, and 22.7 percent bear this out. At an average strain of 22.7 percent the maximum temperature at the center equals 92 percent of the presumed melting temperature of the material. The isotherms are quite narrow in the vertical direction and progressively become narrower as the deformation localizes.

Figure 3 depicts the v_1-velocity field in the reference configuration of the block at average strains of 0 percent, 18.5 percent, 20.8 percent, and 22.7 percent. Because of the initial temperature bump, the deformation becomes nonhomo-

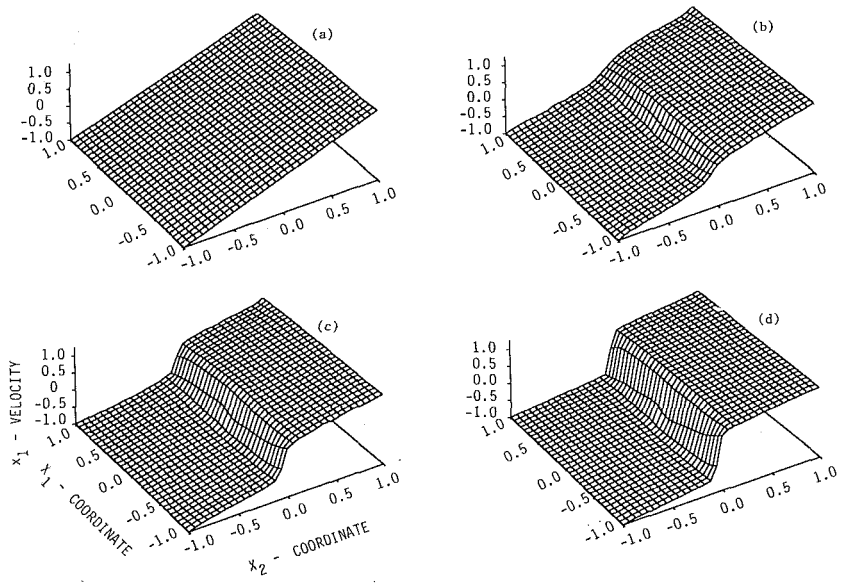

Fig. 3 Velocity field in the direction of shearing at several values of the average strain; (a) $\gamma_{avg}=0$, (b) $\gamma_{avg}=0.185$, (c) $\gamma_{avg}=0.208$, and (d) $\gamma_{avg}=0.227$

geneous. This nonuniformity becomes perceptible at an average strain of 18.5 percent and is quite noticeable when the average strain equals 20.8 percent and 22.7 percent. The nonhomogeneity in the deformation at the corners is not noticeable in these plots probably because of the scale chosen to plot the data. The v_1-velocity field appears to stay antisymmetric in x_2 even through the localization of the deformation. At an average strain of 20.8 percent the shearing strain rate at the center is noticeably higher than what it is within the region $|x_2| \geq 0.1$. During the ensuing deformations of the block, the region near the center undergoes intense straining and that outside of the domain $|x_2| \leq 0.1$ deforms at a strain rate much smaller than the imposed strain rate of 5000 $\sec^{-1}$. With a finer mesh one could sharpen a bit more the boundaries of the two domains.

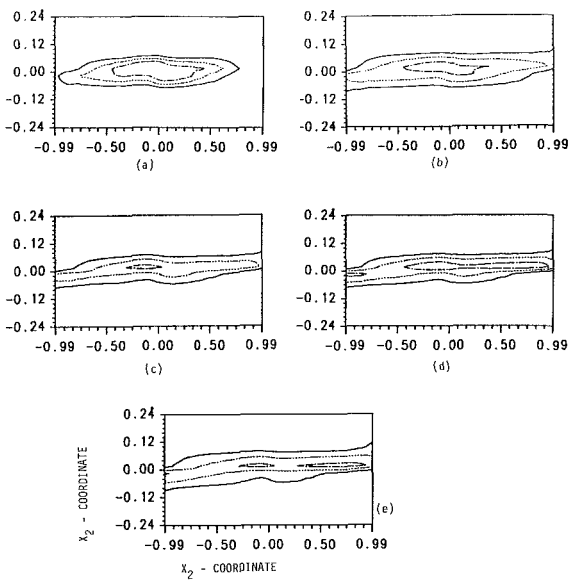

Fig. 4 Contours of the second invariant I of the deviatoric strain rate tensor at different values of the average strain; (a) $\gamma_{avg} = 0.185$, $I_{max} = 3.47$; — 1.5, · · · · · · 2.0, —·—·—· 3.5, (b) $\gamma_{avg} = 0.198$, $I_{max} = 4.45$; — 1.5, · · · · · · 2.5, —·—·—· 3.5, (c) $\gamma_{avg} = 0.208$, $I_{max} = 5.51$; — 2.5, · · · · · · 3.75, —·—·—· 5.0, (d) $\gamma_{avg} = 0.215$, $I_{max} = 6.23$; — 2.5, · · · · · · 3.75, —·—·—· 5.0, and (e) $\gamma_{avg} = 0.227$, $I_{max} = 8.45$; — 2.5, · · · · · · 5.0, —·—·—· 7.5

In Fig. 4 we have plotted the contours of the second invariant I of the deviatoric strain rate tensor $\tilde{\mathbf{D}}$ at different stages of the localization process. At an average strain of 18.5 percent the peak value of I equals 3.47 and it equals 4.45 when the average strain is 19.8 percent. We note that these are plotted in the reference configuration. It is clear that during the deformation of the block from 18.5 percent average strain to 19.8 percent average strain, the contour of $I = 2.5$ has spread out horizontally and become narrower in the vertical direction. The various plots in Fig. 4 give the impression that there is a kind of source term for I at the center. Once the deformation has started to localize, contours of successively higher values of I seem to originate at the center and fan out. They spread out in the direction of shearing. As noted earlier, severe deformations of the block occur now in this narrow region.

Figure 5 depicts the distribution of the effective stress s_e, defined as being equal to the right-hand side of equation (12) within the block at average strains of 0 percent, 18.5 percent, 20.8 percent, and 22.7 percent. Initially it looks like an inverted hat because every material point is assumed to lie on its yield surface. We note that for the simple shearing problem being studied, σ_{12} is the only component of stress having significant values. Because of the higher temperature at points near the center, the flow stress there is reduced. As the body continues to be deformed, the stress distribution within the block, and especially in the region surrounding the center of the block, alters. The nonhomogeneity of the deformation near the corners is now evident. The temperature rise within the block reduces the flow stress needed to deform the material. Consequently, the value of s_e drops at all points. Even though the strain rate invariant I assumes very high values at points within the region of localization, the softening caused by the temperature rise exceeds the hardening due to strain rate effects and the stress drop in the severely deforming region is enormous. For very high rate of drop of s_e, an unloading elastic wave emanates outwards from the shear band (Batra and Kim, 1989). No such unloading wave was observed in this case. It could be due to the coarseness of the mesh, the integration scheme used, or the rate of the drop of s_e was not too high.

The deformed mesh at average strain of 22.7 percent is shown in Fig. 6. The relatively severe deformations within the region of localization, and nonuniformity of deformations near the corners, is evident.

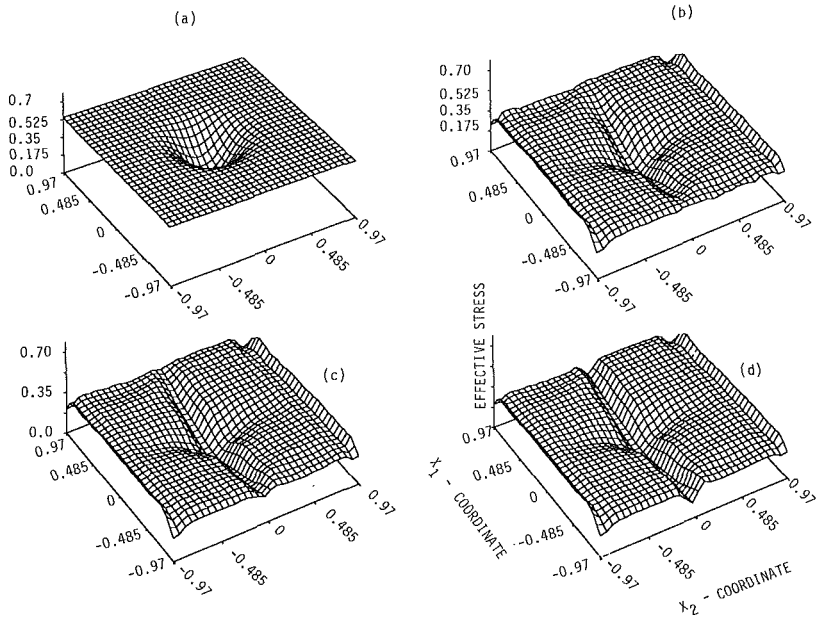

Fig. 5 Distribution of the effective stress within the block at different values of the average strain; (a) $\gamma_{avg} = 0$, (b) $\gamma_{avg} = 0.185$, (c) $\gamma_{avg} = 0.208$, and (d) $\gamma_{avg} = 0.227$

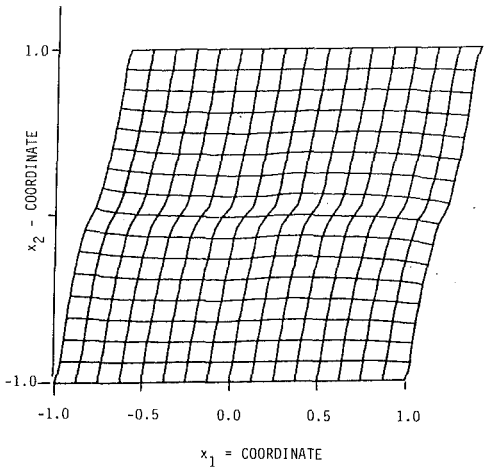

Fig. 6 Deformed mesh at an average strain of 0.227 (simple shearing deformations of the block)

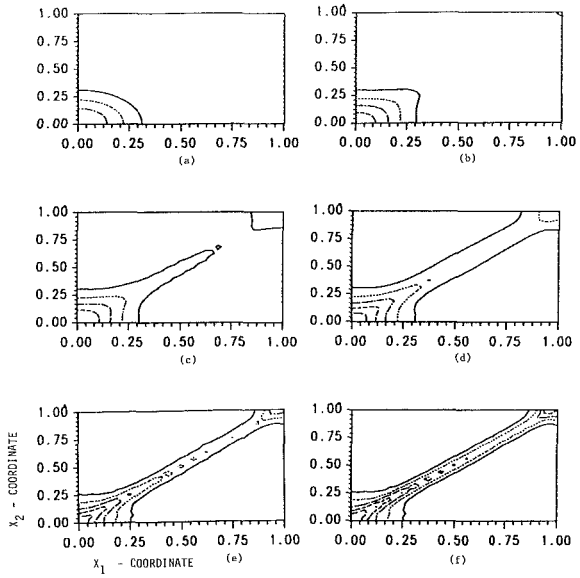

Fig. 7 Isotherms plotted in the reference configuration at different values of the average compressive strain; (*a*) $\gamma_{avg} = 0.0$, $\theta_{max} = 0.2$, — 0.05, • • • • 0.10, —•—•—• 0.15, (*b*) $\gamma_{avg} = 0.035$, $\theta_{max} = 0.286$, — 0.10, • • • • 0.15, —•—•—• 0.20, - - - - 0.25, (*c*) $\gamma_{avg} = 0.040$, $\theta_{max} = 0.313$, see part (*b*) for values of θ corresponding to different curves, (*d*) $\gamma_{avg} = 0.045$, $\theta_{max} = 0.353$, — 0.10, • • • • • 0.15, —•—•—• 0.20, - - - - 0.25, — — — 0.30, (*e*) $\gamma_{avg} = 0.055$, $\theta_{max} = 0.426$, — 0.15, • • • • • 0.20, —•—•—• 0.25, - - - - 0.30, — — — 0.35, and (*f*) $\gamma_{avg} = 0.059$, $\theta_{max} = 0.449$, (see part (*e*) for values of θ corresponding to different curves)

(*b*) ***Results for the Compression Problem.*** Because of the assumed symmetry of the deformation field, the deformations of the block within the first quadrant are analyzed. Several trial runs without introducing any temperature perturbation yielded the following values of the steady-state solution:

$$v_1 = 0.37x_1,\ v_2 = -x_2 \tag{29}$$

for an average applied strain rate of 5000 $\sec^{-1}$. Subsequently this velocity field, and the temperature field given by equation (28), were taken as the initial conditions and the initial boundary value problem solved. A closer look at the results computed by Batra (1987a, 1987b) for the one-dimensional simple shearing problem reveals that the initial state where the perturbation is introduced has very little effect, if any, on the qualitative nature of the results. Figure 7 depicts the

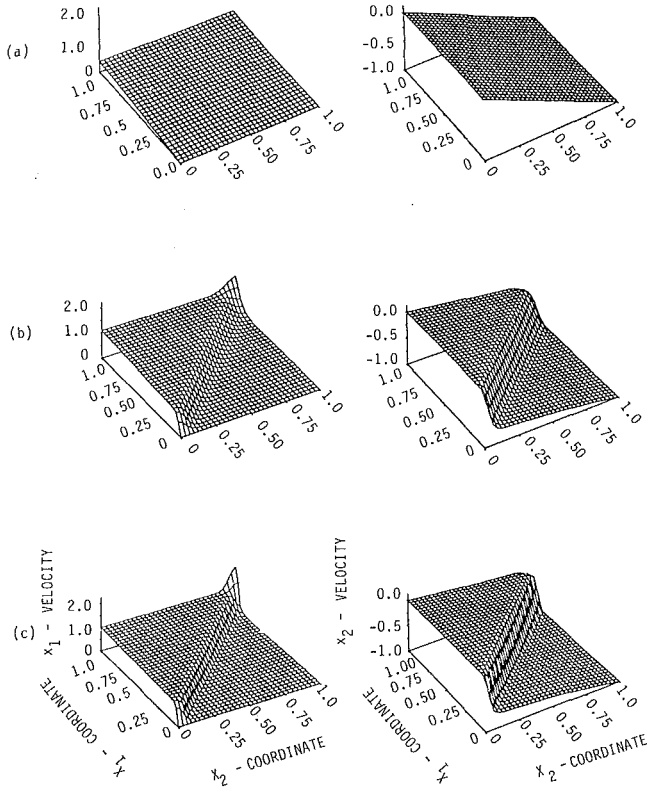

Fig. 8 Velocity field within the block at different values of the average compressive strain; (*a*) $\gamma_{avg} = 0$, (*b*) $\gamma_{avg} = 0.045$, (*c*) $\gamma_{avg} = 0.059$

temperature distribution at several values of the average compressive strain. At an average strain of 3.5 percent the isotherms have changed in shape from elliptic to rhombus and the peak temperature at the center has risen from 0.20 to 0.286. Because of the nonhomogeneous deformations near the top right corner, the temperature rise there is more than that at other points within the block except, of course, those near the center which are undergoing severe deformations. As the temperature plots at average compressive strains of 4 percent, 4.5 percent, 5.5 percent, and 5.9 percent show vividly, the isotherms spread out diagonally indicating that the material around the main diagonal is deforming severely. At these average strains the peak temperature occurs at the center and equals 0.313, 0.353, 0.426, and 0.449, respectively. Thus, the rate of temperature rise at the center is small initially, increases as the deformation begins to localize, and tapers off during the late stages of the localization. Even though heat is being conducted out of this central region the heat produced due to the plastic dissipation exceeds that lost due to conduction. Once the localization process is initiated, the heat generated due to plastic working becomes quite high and the rate of temperature rise within the central region picks up. However, the stress required to deform the material drops and thus reduces the energy dissipated due to plastic working. This and the heat conducted out of the central hotter region explains the slow rate of temperature rise during the late stages of the localization of the deformation.

In Fig. 8 we have plotted the v_1- and v_2-velocity fields at average strains of 0, 4.5 percent, and 5.9 percent. Except at points around the diagonal passing through the top right corner, both v_1 and v_2 vary slowly and nearly linearly, thereby implying that the material region within a narrow zone on both sizes of the diagonal line is undergoing severe deformations. Figure 9 shows the contours of the second invariant I of the deviatoric strain rate tensor at average compressive strains

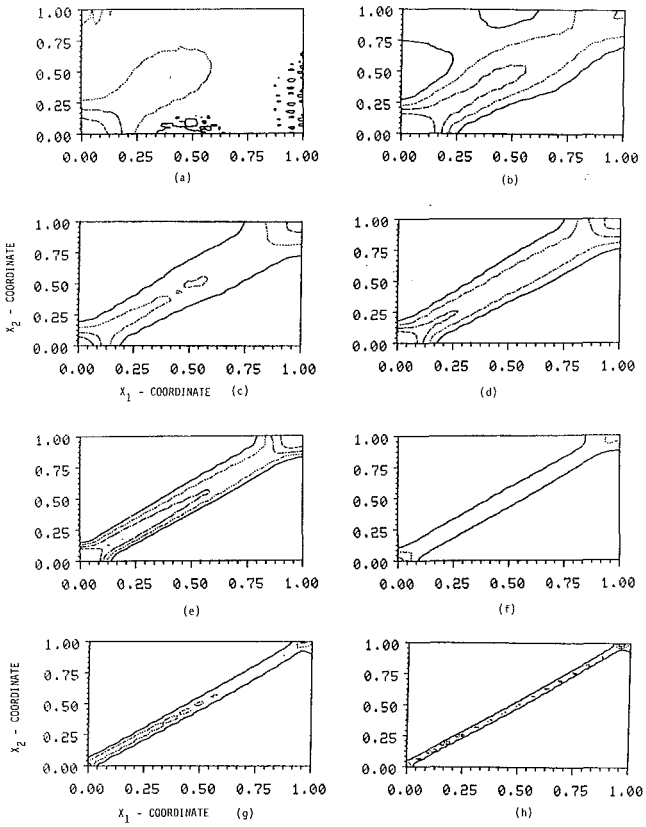

Fig. 9 Contours of the second invariant I of the deviatoric strain rate tensor at different values of the average compressive strain; (*a*) $\gamma_{avg} = 0.012$, $I_{max} = 2.0$. — 1.0, • • • • • • 1.25, —•—•—• 1.50, - - - - 1.75, (*b*) $\gamma_{avg} = 0.018$, $I_{max} = 2.53$, — 1.0, • • • • • • 1.25, —•—•—• 1.50, - - - - 1.75, (*c*) $\gamma_{avg} = 0.025$, $I_{max} = 2.95$. — 1.0, • • • • • • 1.5, —•—•—• 2.0, - - - - 2.5, (*d*) $\gamma_{avg} = 0.03$, $I_{max} = 3.70$, see part (*c*) for values of I corresponding to different curves, (*e*) $\gamma_{avg} = 0.035$, $I_{max} = 5.53$, — 1.5, • • • • • • 2.0, —•—•—• 2.5, - - - - 3.0, (*f*) $\gamma_{avg} = 0.040$, $I_{max} = 8.73$, — 2.5, • • • • • • 5.0, —•—•—• 7.5, (*g*) $\gamma_{avg} = 0.053$, $I_{max} = 16.92$, — 2.5, • • • • • • 7.5, —•—•—• 12.5, and (*h*) $\gamma_{avg} = 0.059$, $I_{max} = 20.7$, — 7.5, • • • • • • 12.5, —•—•—• 17.5

of 0.012, 0.018, 0.025, 0.03, 0.035, 0.04, 0.055, and 0.059. As for the simple shearing problem, the maximum value of I occurs at points near the center of the block and these contours seem to originate at the center and spread out along and perpendicular to the direction of maximum shearing strain; their speed probably depends upon the mesh size. Also, the width of the severely deforming region depends upon the mesh size, too.

Figure 10 depicts the distribution of the effective stress s_e at average strains of 0, 0.027, 0.045, and 0.059. Initially the stress is uniform everywhere except in a narrow region near the center where the flow stress has been reduced due to the higher value of the temperature at these points. The plot at $\gamma_{avg} = 0.027$ reveals that the flow stress has dropped everywhere due to the rise in the temperature of material particles. Still, the effective stress is uniformly distributed except at points near the center of the block. It seems that the localization of the deformation begins in earnest at $\gamma_{avg} = 0.045$. At $\gamma_{avg} = 0.059$ the material region around the main diagonal has severely deformed. The deformed mesh for $\gamma_{avg} = 0.059$ is shown in Fig. 11. That the band has formed is difficult to visualize from the deformed mesh shown. Also, the mesh is incapable of resolving sharp deformation gradients within the localized region.

5 Discussion and Conclusions

The 9-noded quadrilateral element used herein seems to have performed satisfactorily as far as the initiation and some growth of the adiabatic shear band is concerned. As for computations with one-dimensional problems (Batra, 1987a; Batra and Kim, 1989), it is probably due to the coarseness of the mesh that sharp gradients of the deformation within the region of localization could not be completely resolved. This is also supported by the recent work of Shuttle and Smith (1988) on the numerical simulation of shear band formation in soils. Both for plane strain, simple shearing deformations of the block and plane strain compression of the block, the shear band is formed along the direction of maximum shearing. For the compression problem the shear band formed at an average strain of 0.059, and for the simple shearing problem it formed when the average strain equaled 0.229. The results computed

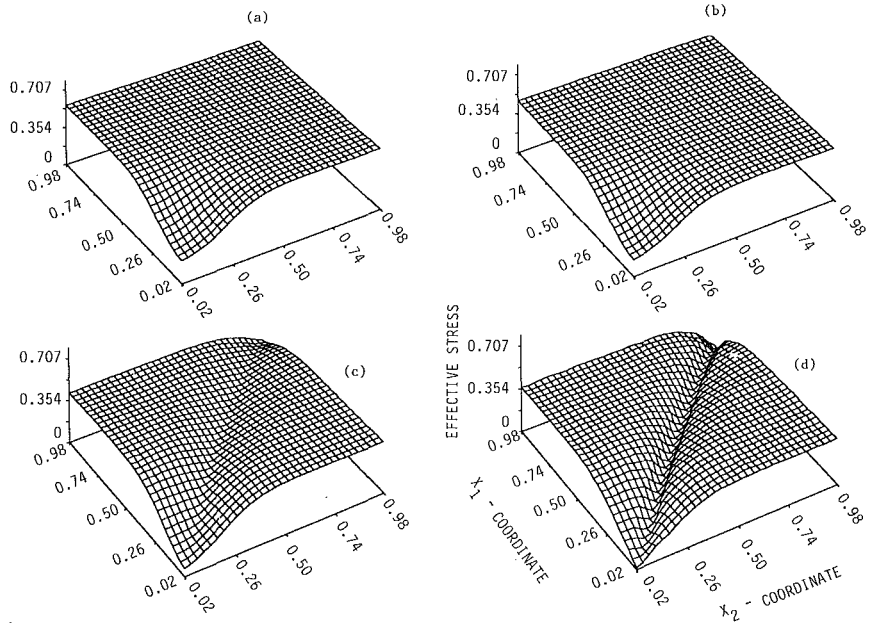

Fig. 10 Distribution of the effective stress within the block at different values of the average strain; (*a*) $\gamma_{avg} = 0$, (*b*) $\gamma_{avg} = 0.027$, (*c*) $\gamma_{avg} = 0.045$, and (*d*) $\gamma_{avg} = 0.059$

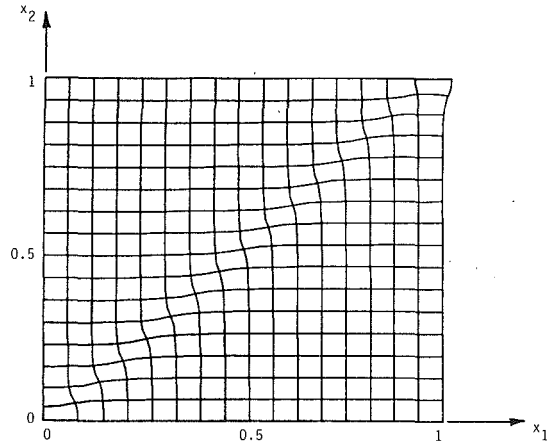

Fig. 11 Deformed mesh at an average compressive strain of 0.059

herein are in qualitative agreement with those of Needleman (1989). Because of the different constitutive assumptions made and the difference in modeling a material inhomogeneity, it is hard to make any quantitative comparisons.

Acknowledgments

This work was supported by the U.S. National Science Foundation grant MSM-8715952 and the U.S. Army Research Office Contract DAAL03-88K-0184 to the University of Missouri-Rolla.

References

Bai, Y. L., 1981, "A Criterion for Thermoplastic Shear Instability," *Shock Waves and High Strain-Rate Phenomena in Metals*, M. A. Myers, and L. E. Murr, eds., Plenum Press, New York, pp. 277–283.

Batra, R. C., 1987a, "The Initiation and Growth of, and the Interaction Among Adiabatic Shear Bands in Simple and Dipolar Materials," *Int. J. Plasticity*, Vol. 3, pp. 75–89.

Batra, R. C., 1988, "Steady State Penetration of Thermoviscoplastic Targets," *Comp. Mech.*, Vol. 3, pp. 1–12.

Batra, R. C., and Kim, C. H., 1989, "Adiabatic Shear Banding in Elastic-Viscoplastic Nonpolar and Dipolar Materials," *Int. J. Plasticity*, Vol. 5, to appear.

Batra, R. C., and Lin, Pei-Rong, 1989, "Steady State Axisymmetric Deformations of a Thermoviscoplastic Rod Striking a Hemispherical Rigid Cavity," *Int. J. Impact Engng.*, Vol. 8, to appear.

Bell, J. F., 1968, *Physics of Large Deformations of Crystalline Solids*, Springer-Verlag, New York.

Bodner, S. R., and Partom, Y., 1975, "Mechanical Properties at High Rate of Strain," *Inst. Phys. Conf.*, Ser. No. 21, pp. 102–110.

Burns, T. J., 1985, "Approximate Linear Stability Analysis of a Model of Adiabatic Shear Band Formation," *Q. Appl. Math.*, Vol. 43, pp. 65–84.

Clifton, R. J., 1980, "Adiabatic Shear in Material Response to Ultrahigh Loading Rates," U.S. NRC National Material Advisory Board Report NMAB-356, W. Herrman et al., eds.

Clifton, R. J., Duffy, J., Hartley, K. A., and Shawki, T. G., 1984, "On Critical Conditions for Shear Band Formation at High Strain Rates," *Scripta Metall.*, Vol. 18, pp. 443–448.

Costin, L. S., Crisman, E. E., Hawley, R. H., and Duffy, J., 1979, "On the Localization of Plastic Flow in Mild Steel Tubes Under Dynamic Torsion Loading," *Inst. Phys. Conf. Ser.*, Vol. 47, pp. 90–100.

Hughes, T. J. R., 1987, *The Finite Element Method Linear Static and Dynamic Finite Element Analysis*, Prentice-Hall, Englewood Cliffs, N.J.

Lin, M. R., and Wagoner, R. H., 1986, "Effect of Temperature, Strain and Strain-Rate on the Tensile Flow Stress of I. F. Steel and Stainless Steel Type 310," *Scripta Metall.*, Vol. 20, pp. 143–148.

Lindholm, U. S., and Johnson, G. R., 1983, "Strain-Rate Effects in Metals at Large Strain-Rates," *Material Behavior Under High Stresses and Ultrahigh Loading Rates*, J. Mescal, and V. Weiss, eds., pp. 61–79.

Marchand, A., and Duffy, J., 1988, "An Experimental Study of the Formation Process of Adiabatic Shear Bands in a Structural Steel," *J. Mech. Phys. Solids*, Vol. 36, pp. 251–283.

Merzer, A. M., 1983, "Modelling of Adiabatic Shear Band Development from Small Imperfections," *J. Mech. Phys. Sol.*, Vol. 30, pp. 323–338.

Moss, G. L., 1981, "Shear Strain, Strain Rates and Temperature Changes in Adiabatic Shear Bands," *Shock Waves and High Strain-Rate Phenomenon in Metals*, M. A. Meyers and L. E. Murr, eds., Plenum Press, New York, pp. 299–312.

Needleman, A., 1989, "Dynamic Shear Band Development in Plane Strain," ASME Journal of Applied Mechanics, Vol. 56, pp. 1–9.

Rogers, H. C., 1979, "Adiabatic Plastic Deformation," *Ann. Rev. Mat. Sci.*, Vol. 9, pp. 283–311.

Rogers, H. C., 1983, "A Review of Adiabatic Shearing," *Material Behavior Under High Stress and Ultrahigh Loading Rates*, J. Mescall and V. Weiss, eds., Plenum Press, New York, pp. 101–118.

Shuttle, D. A., and Smith, I. M., 1988, "Numerical Simulation of Shear Band Formation in Soils," *Int. J. for Numerical and Analytical Methods in Geomechanics*, Vol. 12, pp. 611–626.

Tillotson, J. H., 1962, General Atomic Report GA-3216.

Timothy, S. P., 1987, "The Structure of Adiabatic Shear Bands in Metals: A Critical Review," *Acta Metall.*, Vol. 35, pp. 301–306.

Wright, T. W., and Batra, R. C., 1985, "The Initiation and Growth of Adiabatic Shear Bands," *Int. J. Plasticity*, Vol. 1, pp. 205–212.

Wright, T. W., and Walter, J., 1987, "On Stress Collapse in Adiabatic Shear Bands," *J. Mech. Phys. Solids*, Vol. 35, pp. 701–716.

Wu, F. H., and Freund, L. B., 1984, "Deformation Trapping Due to Thermoplastic Instability in One-Dimensional Wave Propagation," *J. Mech. Phys. Solids*, Vol. 32, pp. 119–132.

Zener, C., and Hollomon, J. H., 1944, "Effect of Strain-Rate on Plastic Flow of Steel," *J. Appl. Phys.*, Vol. 14, pp. 22–32.

Zienkiewicz, O. C., Onate, E., and Heinrich, J. C., 1981, "A General Formulation for Coupled Thermal Flow of Metals Using Finite Elements," *Int. J. Numer. Methods Eng.*, Vol. 17, pp. 1497–1514.